

**RESEARCH ARTICLE**

# A moisture budget perspective on Australian rainfall variability

Sunil Kumar Pariyar<sup>1</sup>  | Giovanni Liguori<sup>1,2</sup>  | Christian Jakob<sup>1,3</sup> | Martin S. Singh<sup>1,3</sup> | Michael J. Reeder<sup>1,3</sup> | Michael A. Barnes<sup>1,3</sup> 

<sup>1</sup>School of Earth, Atmosphere and Environment, Monash University, Clayton, Victoria, Australia

<sup>2</sup>Department of Biological, Geological, and Environmental Sciences (BIGEA), University of Bologna, Bologna, Italy

<sup>3</sup>ARC Centre of Excellence for Climate Extremes, Sydney, New South Wales, Australia

**Correspondence**

Sunil Kumar Pariyar, School of Earth, Atmosphere and Environment, Monash University, Clayton, VIC, Australia.  
Email: [sunil.pariyar@monash.edu](mailto:sunil.pariyar@monash.edu), [sunilkumar.atmos@gmail.com](mailto:sunilkumar.atmos@gmail.com)

**Funding information**

Australian Research Council,  
Grant/Award Number: DP200102954

**Abstract**

Rainfall variability over Australia is revisited from the viewpoint of the atmospheric moisture budgets in three regions: the extratropics, Subtropics, and Tropics. The budgets are calculated using three-hourly European Centre for Medium-Range Weather Forecasts Reanalysis v5 (ERA5) and ERA5-Land data between 1979 and 2022. The use of the moisture budget at short time-scales enables the investigation of the relationship between synoptic weather-scale processes and the longer term variability of the rainfall climate. The total variability in the vertically integrated moisture flux divergence (VIMD) is significantly larger than the evaporation minus precipitation ( $E - P$ ), to a large extent due to the sub-daily time-scales.  $E - P$  is related more closely to moisture flux convergence in winter (summer) over south (north) Australia, suggesting a clear seasonality in the relationship between the two budget terms. The  $E - P$ -VIMD relationship is nearly in phase in the Tropics, whereas VIMD leads  $E - P$  by 9–15 hr with eastward-propagating signals in the extratropics and Subtropics. Such seasonal and regional discrepancies in the relationship are attributed to the background state of moisture availability and temperature as represented by relative humidity and lifting condensation levels. The variability of the budget imbalance and its seasonality are dominated by the variability in VIMD. The imbalance reduces rapidly with temporal smoothing, with the storage term approaching zero at approximately 20 days, which can be thought of as making a transition time-scale from high-frequency weather-related variability into slow-varying background conditions. Weather-related variability (cyclones, fronts, and thunderstorms) dominates the overall  $E - P$  variability in the extratropics and Subtropics, whereas slow-varying background conditions contribute equally to the total variability in the Tropics.

**KEYWORDS**

analysis, climate, dynamic/processes, physical phenomenon, rainfall, scale, seasonal, synoptic, tools and methods

This is an open access article under the terms of the [Creative Commons Attribution](https://creativecommons.org/licenses/by/4.0/) License, which permits use, distribution and reproduction in any medium, provided the original work is properly cited.

© 2024 The Author(s). *Quarterly Journal of the Royal Meteorological Society* published by John Wiley & Sons Ltd on behalf of Royal Meteorological Society.

## 1 | INTRODUCTION

The rainfall variability in Australia is commonly attributed to the combined influence of large-scale modes of variability and various weather systems. Planetary-scale factors, such as El Niño–Southern Oscillation, Indian Ocean dipole, interdecadal Pacific oscillation, Madden–Julian oscillation, and southern annular mode, are thought to regulate much of the rainfall variability from subseasonal to decadal time-scales (Ashok *et al.*, 2003; Chiew *et al.*, 1998; Cowan *et al.*, 2013; Hendon *et al.*, 2007; Liguori *et al.*, 2022; Power *et al.*, 1999; Risbey *et al.*, 2009; Spensberger *et al.*, 2020). On shorter time and space scales, weather systems such as fronts, thunderstorms, cyclones, and tropical lows are common rain-producing systems (Dowdy & Catto, 2017; Pepler *et al.*, 2020, 2021). The temporal and spatial variability of regional rainfall depends primarily on the interaction between these high-frequency weather systems and slowly evolving large-scale climate modes. It is commonly argued that the dominant modes of variability affect the occurrence of regional rainfall in Australia by modifying the large-scale atmospheric circulation and thereby modifying the frequency, intensity, and location of rain-bearing weather systems. It is, therefore, important to explore how rainfall variability on weather and climate time-scales interact.

The atmospheric moisture budget is a useful theoretical framework to connect weather and climate scales (Chen *et al.*, 2019; Norris *et al.*, 2019a; Norris *et al.*, 2019b; Norris *et al.*, 2020; Seager *et al.*, 2014; Ting *et al.*, 2018), as it links the precipitation  $P$  variability to two variables: evaporation  $E$  and moisture divergence in the form of net fluxes as expressed by the following equation (Trenberth & Guillemot, 1995):

$$\frac{\partial q}{\partial t} + \nabla \cdot \langle q\mathbf{V} \rangle = E - P, \quad (1)$$

where  $q$  ( $\text{g}\cdot\text{kg}^{-1}$ ) is the specific humidity and  $\mathbf{V} = (u, v)$  ( $\text{m}\cdot\text{s}^{-1}$ ) is the zonal and meridional wind. The angle brackets represent a mass-weighted vertical integral. The term on the right-hand side is the difference between surface evaporation and precipitation ( $E - P$ ). The first term on the left-hand side is the tendency of column-integrated moisture, also known as the storage term, and the second term is the vertically integrated moisture divergence (VIMD). Through Equation (1), changes in the vertically integrated moisture content in a region are related to fluxes to and from other areas (remote and mostly circulation driven) and fluxes to and from the surface (local and mostly thermodynamically driven).

On sufficiently longer time-scales, the meaning of which will be discussed in the next section, the climate

system can be assumed to be at equilibrium. Thus, the storage term, a temporal derivative, approaches zero and  $E - P$  is balanced by VIMD, suggesting a direct connection between large-scale circulation and thermodynamic and dynamic processes within the column. However, on short weather time-scales, the balance usually does not hold. As the dynamical fluxes from other areas are produced primarily by weather systems entering or leaving the regions, exploring how this balance is achieved in different regions as the averaging intervals vary can potentially provide insight into how weather systems interact with long-term climate variability. However, the distinction between high-frequency weather processes and slow varying climate variability in terms of time-scale is not documented for Australia. Here, we present an approach to quantify the weather–climate transition time-scale. The climate time-scale in this study represents the low-frequency variability longer than a time-scale where the two budget terms are in balance.

Previous studies on rainfall variability in Australia have focused on understanding how large-scale climate modes are related to rainfall variability (Ashok *et al.*, 2003; Ashok *et al.*, 2007; Cowan *et al.*, 2013; Fierro & Leslie, 2013; Li *et al.*, 2016; Liguori *et al.*, 2022; Lim *et al.*, 2017; Risbey *et al.*, 2009), how different weather systems affect rainfall variability (Dowdy & Catto, 2017; Hauser *et al.*, 2020; Moron *et al.*, 2019; Pepler *et al.*, 2020, 2021; Wilson *et al.*, 2013), and how rainfall variability will evolve in the near future under different climate change scenarios (Alexander & Arblaster, 2017; Brown *et al.*, 2016; Brown *et al.*, 2017; Dey *et al.*, 2019; Grose *et al.*, 2020; Narsey *et al.*, 2020; Pitman & Perkins, 2008; Zhang *et al.*, 2019). However, little attention has been given to understanding how rainfall variability on the weather time-scale connects to climate. Also, studies on rainfall variability in Australia based on the moisture budget are scarce (Holgate *et al.*, 2020; Newman *et al.*, 2012; Norris *et al.*, 2022). In this context, this study investigates how dynamical processes, as represented by VIMD, are related to rainfall variability and how such variability on weather time-scales relates to and integrates with climate variability.

This article investigates the moisture budget over three Australian regions representative of the extratropics, Subtropics, and Tropics, with a focus on how and on what time-scales the balance between  $E - P$  and large-scale fluxes is achieved through weather variability. This leads us to a novel separation between weather and climate time-scales based on the behaviour of the moisture budget. We show that different regions have very different contributions from weather versus climate variability and different relationships between the different budget components. Finally, the new framework developed here is

applied to understanding the processes leading to anomalously wet and dry years in the different regions.

## 2 | DATA AND METHODS

Throughout this study, we use three-hourly data from the European Centre for Medium-Range Weather Forecasts Reanalysis v5 (ERA5; Hersbach *et al.*, 2020) at  $0.25^\circ \times 0.25^\circ$  resolution for the years 1979 to 2022. Specifically, we use rainfall, evaporation, vertically integrated moisture flux divergence, mean-sea-level pressure (MSLP), specific humidity  $q$ , and wind divergence data. The VIMD in ERA5 is computed from model levels by integrating the horizontal rate of moisture flow per metre across the flow for a column of air extending from the surface to the top of the atmosphere. For the evaporation over land, we use the data from the ERA5-Land analysis (Muñoz-Sabater *et al.*, 2021), as it provides a higher quality representation of the land surface consistent with the atmospheric conditions depicted by ERA5. For any ocean areas, we use evaporation directly from ERA5. As rainfall can strongly vary seasonally across the Australian continent, we separate our analysis into extended summer (October–March) and extended winter (April–September) seasons. We only show the results for summer in the Tropics, as there is very little (less than 20%) rainfall in winter, at least over land (Suppiah, 1992).

The budget terms ( $E - P$  and VIMD) are calculated by taking the area-weighted average over three representative regions of the same size in Australia with climatologically high rainfall rates: one in the extratropics, one in the Subtropics, and one in the Tropics (Figure 1). We estimate the storage term by subtracting VIMD from  $E - P$ , which might include some numerical error from the reanalysis (Mayer *et al.*, 2021). To quantify this, the correlation coefficients and root-mean-square error between the estimated and actual storage terms are computed. The actual storage term is computed by taking the 3-hr difference of the vertically integrated specific humidity. The actual storage term shows good correspondence with the estimated one, with correlation coefficients (root-mean-square error) of 0.93 (0.31 mm), 0.90 (0.3 mm), and 0.89 (0.31 mm) for the extratropics, Subtropics, and Tropics respectively, based on three-hourly time series. When we repeat all the analyses presented here using the actual storage term instead of the estimated storage term, the results are similar and, therefore, do not change any of our major conclusions. For convenience, we refer to the storage terms as residual in subsequent sections.

To quantify the contribution of specific humidity and wind divergence to total VIMD, we compute the total column moisture by integrating the specific humidity from

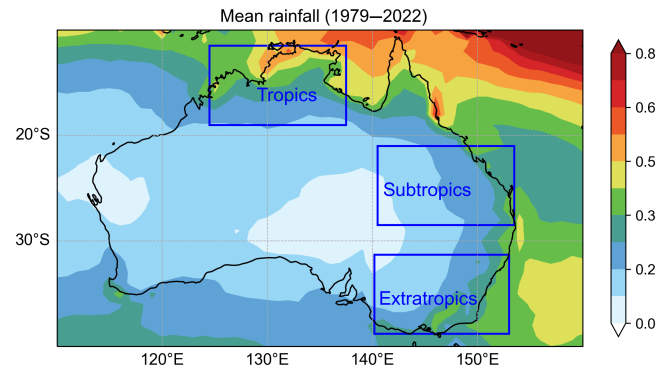


**FIGURE 1** Rainfall climatology (mm/3 hr) between 1979 and 2022. The blue boxes define the study region in the extratropics ( $31^\circ\text{S}$ – $38.5^\circ\text{S}$ ,  $140^\circ\text{E}$ – $153^\circ\text{E}$ ), Subtropics ( $21^\circ\text{S}$ – $29^\circ\text{S}$ ,  $140.5^\circ\text{E}$ – $153.5^\circ\text{E}$ ), and Tropics ( $12^\circ\text{S}$ – $19.5^\circ\text{S}$ ,  $124.5^\circ\text{E}$ – $137.5^\circ\text{E}$ ).

1,000 to 1 hPa. Likewise, we calculate the lower tropospheric wind divergence by integrating horizontal divergence from 1,000 to 850 hPa, as the column-integrated values are close to zero. We integrate only up to 850 hPa, as the climatological specific humidity is mostly concentrated in the lower troposphere. Note that both vertical integrals are mass weighted.

We use six-hourly Australian weather types datasets from 1979 to 2015 (Pepler *et al.*, 2020) to assess the contribution of different weather systems to rainfall variability. The weather types dataset objectively identifies the occurrence of fronts, cyclones, thunderstorms, and their combinations based on ERA-Interim reanalysis at  $0.75^\circ$  horizontal resolution. The dataset identifies eight weather types using various methods: cyclone only, front only, thunderstorm only, cyclone–front, cyclone–thunderstorm, front–thunderstorm, cyclone–cold front–thunderstorm, unconfirmed front/cyclone (fronts or cyclone identified by only one method), and undefined (no weather system is defined). Readers are referred to Pepler *et al.* (2020) for more details. Even though the data are available for the entire Australian continent, the weather types identified are mostly useful for areas south of  $25^\circ\text{S}$  as the techniques used for cyclones and fronts identification are more effective for midlatitude weather systems (Pepler *et al.*, 2020). Therefore, we use this dataset only for extratropics and subtropics.

For the Tropics, we use a six-hourly coherent potential vorticity (PV) minimum to represent the weather processes. Coherent cyclonic PV anomalies were tracked on the 315 K isentropic surface using the algorithm of Barnes *et al.* (2023) based on six-hourly ERA5 data. Only closed cyclonic PV minima with a minimum threshold of 0.01 PVU ( $1 \text{ PVU} = 1 \times 10^{-6} \text{ K}\cdot\text{m}^2\cdot\text{kg}\cdot\text{s}^{-1}$ ) that persist for at least 24 hr are retained by the algorithm. Low-level

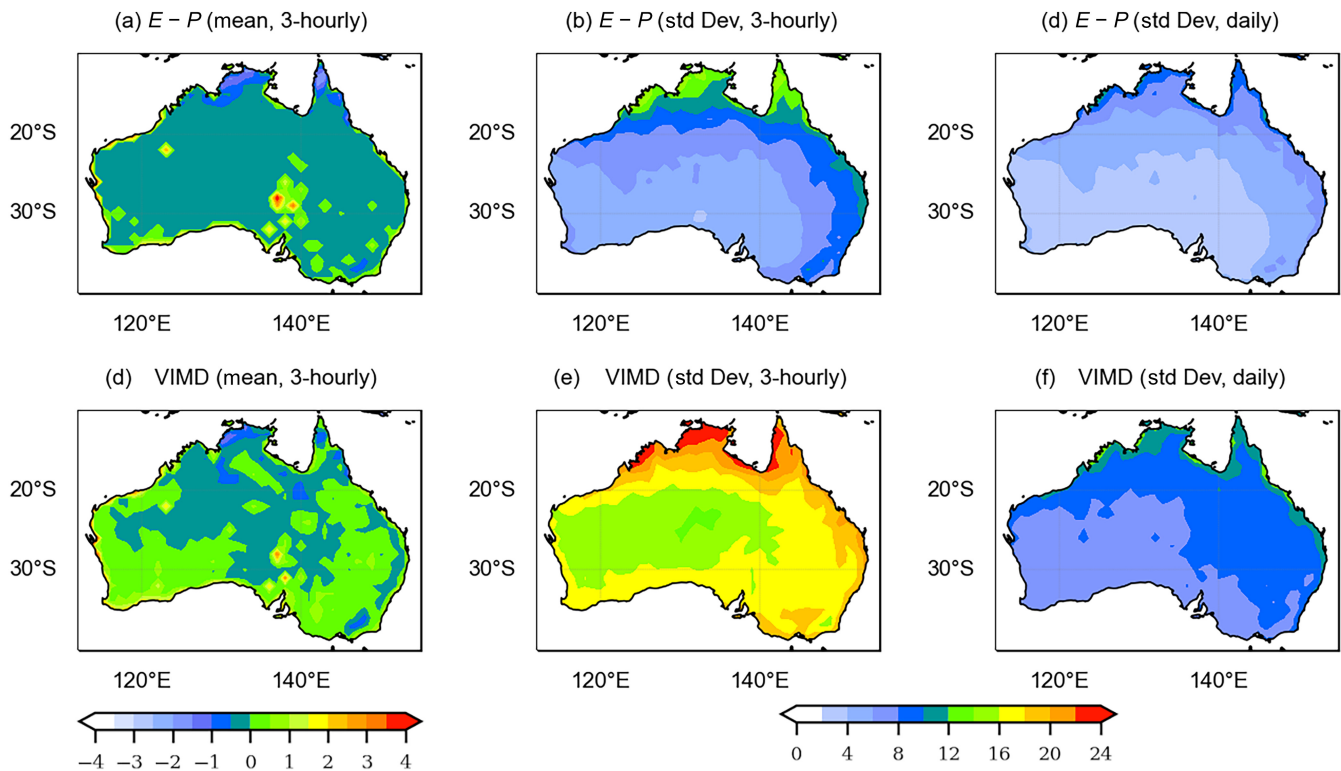


**FIGURE 2** (a, d) Mean and (b, e) standard deviations of  $E - P$  and vertically integrated moisture flux divergence (VIMD) (mm/3 hr) based on three-hourly data between 1979 and 2022. (d, f) Standard deviations based on 1-day running mean. Positive values of VIMD represent moisture flux divergence.

(in this case 315 K) coherent cyclonic PV anomalies are found preferentially in the Australian Tropics and along the east coast of the continent during the summer months (Berry *et al.*, 2012; Hoang *et al.*, 2016). They are important for the rainfall over the Australian monsoon, with an estimated 40–50% of the rainfall occurring in tropical Australia occurring in proximity to them (Berry *et al.*, 2012).

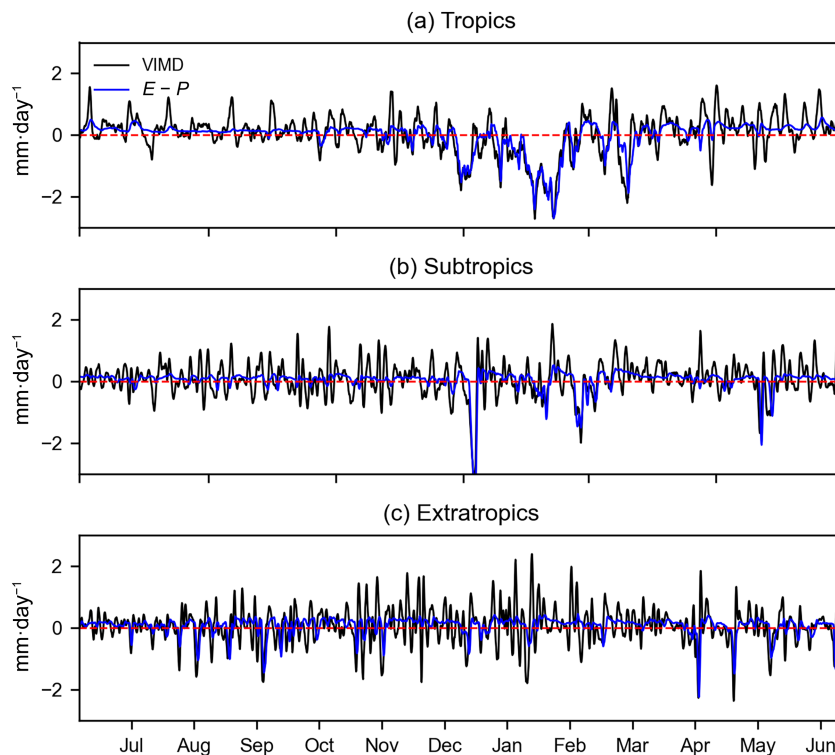
## 2.1 | Overall moisture budget key characteristics

To provide an overview of the spatial distribution of the moisture budget, Figure 2 shows the mean and standard deviation of  $E - P$  and VIMD between 1979 and 2022. We note that the climatology of the three-hourly  $E - P$  and VIMD is not in perfect balance. Regions with larger imbalances are associated with complex topography, such as the inland regions of southeast and southwest Australia (Figure 2a,d), where the numerical error is the largest for VIMD in the ERA5 dataset (Mayer *et al.*, 2021). Though the spatial structures of the standard deviation based on three-hourly data are similar for  $E - P$  and VIMD, with larger variability along the coasts and smaller variability inland, their magnitudes differ significantly

(Figure 2b,e). The standard deviation for VIMD is nearly twice that of  $E - P$ . Applying a daily running mean filter to the three-hourly time series removes the large difference in variability between the two budget components (Figure 2c,f). This indicates that the difference in variability is to a large extent due to the higher sub-daily variability of VIMD. It is noteworthy that both  $E - P$  and VIMD show larger variability along the northern and eastern coastlines because of the relatively larger wind and moisture variability associated with the land–ocean interaction (Mapes *et al.*, 2003). However, over the south and southwest coasts and associated land masses, the variability of  $E - P$  and VIMD is comparatively low as the annual climatological winds are predominantly northeasterlies to easterlies (Pepler *et al.*, 2018) flowing from land areas, and hence are relatively dry. The seasonal maps of mean and variability exhibit similar characteristics (Supporting Information Figure S1).

To illustrate the difference in variability of  $E - P$  and VIMD in the three regions at different times of the year, the daily time series from July 1979 to June 1980 is presented in Figure 3. There is a clear seasonal contrast in the covariance of the budget terms, and consequently the budget closure, between the extratropics and Tropics. In the extratropics, the two budget terms are more closely related in winter than in summer with the covariance

**FIGURE 3** Daily time series of  $E - P$  and vertically integrated moisture flux divergence (VIMD) in  $\text{mm}\cdot\text{day}^{-1}$  from July 1979 to June 1980 in the (a) Tropics, (b) Subtropics, and (c) extratropics. The daily values are obtained by applying a 1-day running mean to three-hourly time series. Positive values of VIMD represent divergence.



of  $0.08$  and  $0.02 \text{ mm}^2\cdot\text{day}^{-2}$ , whereas the opposite is true in the Tropics ( $\text{COV}_{\text{summer}} \sim 0.37 \text{ mm}^2\cdot\text{day}^{-2}$ ;  $\text{COV}_{\text{winter}} \sim 0.02 \text{ mm}^2\cdot\text{day}^{-2}$ ).

The seasonal evolution of budget terms in the Subtropics is a mix of the other two regions: the budget terms co-vary more in summer ( $\text{COV}_{\text{summer}} \sim 0.18 \text{ mm}^2\cdot\text{day}^{-2}$ ;  $\text{COV}_{\text{winter}} \sim 0.02 \text{ mm}^2\cdot\text{day}^{-2}$ ), like in the Tropics, and the seasonal evolution of the VIMD variability is like that of the extratropics. This is because the rainfall variability in the Subtropics is affected by both extratropical disturbances (e.g., atmospheric blocking and cut-off lows) and tropical processes (e.g., tropical cyclones, and local trade wind variability) (Klingaman, 2012). We will quantify the covariance of the moisture budget components in Section 2.3. First, we will investigate the characteristics of their variance in the following section.

## 2.2 | Moisture budget variability

### 2.2.1 | The seasonal cycle of variability

The single year of the time evolution of the budget terms (Figure 3) showed a clear seasonality in the imbalance, with marked differences in the seasonal evolution for different regions. We quantify this behaviour by investigating the seasonality of the mean and variance of the imbalance (residual term) in the budget. The primary reason for focusing on the residual term is to assess the seasonal evolution of moisture imbalance.

The seasonal evolution of the mean and variance of the residual shows remarkable differences between the extratropics and Tropics, with the Subtropics showing the behaviour of both regions (Figure 4). Climatologically, the extratropics experience a moisture decrease for most months except for spring (Figure 4c, green plus signs). As monthly  $E - P$  is mostly positive in the extratropics (not shown), the moisture deficit is primarily due to increased large-scale moisture divergence. In contrast, there is an increase (decrease) in moisture from spring to summer (fall to winter) in the Tropics (Figure 4a) because of an increase (decrease) in both evaporation and moisture convergence (not shown). The seasonal cycle of the mean residual in the Subtropics resembles that of the extratropics (Figure 4b). The variance of the residual (blue bars) shows pronounced seasonality, with larger (smaller) variability in summer (winter) in the extratropics. The Tropics show a small seasonal cycle in residual variability, while the subtropical values fall between those of the other regions with a small seasonal cycle more closely resembling that of the extratropics.

To quantify the individual contributions of  $E - P$  and VIMD to the total residual variance, we decompose the total variance into three components: (a) the variance contributed by  $E - P$ , (b) the variance contributed by VIMD, and (c) the variance contributed by covariability between  $E - P$  and VIMD, such that their sum is equal to the total variance. Note that the covariance between  $E - P$  and VIMD needs to be subtracted to yield the total residual variance but is presented as positive in the figure

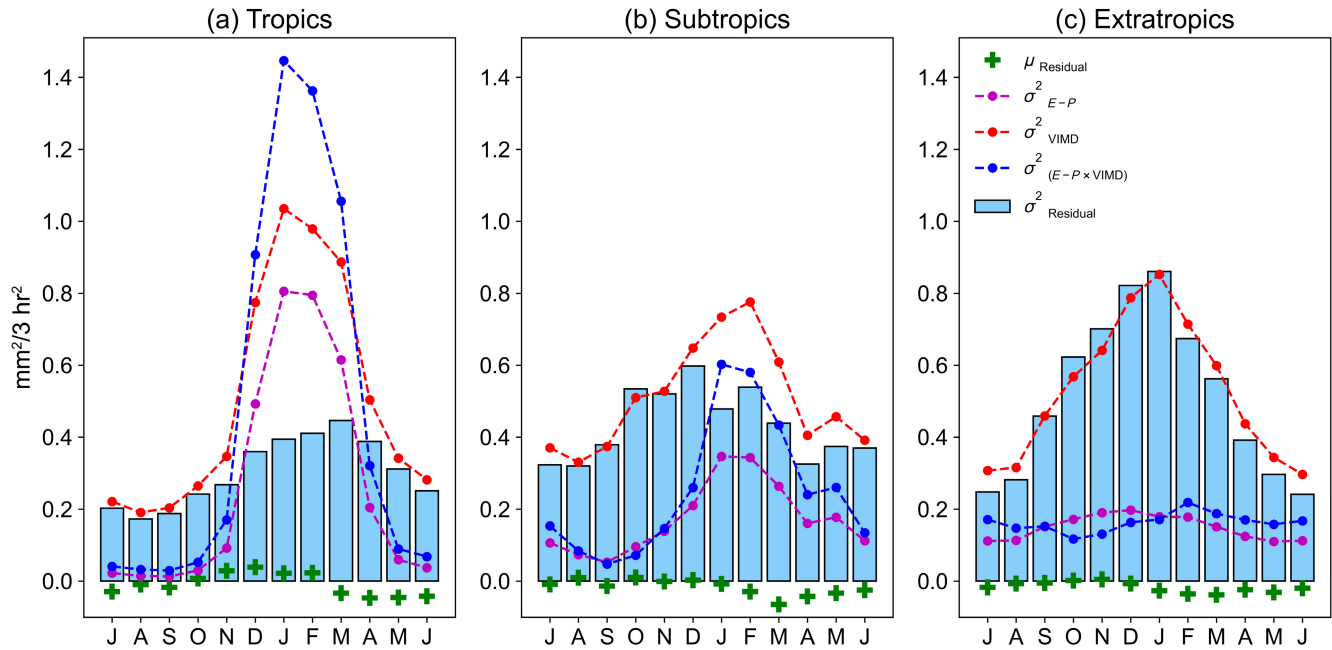


**FIGURE 4** Mean (green plus; mm/3 hr) and variance (light blue bars; mm<sup>2</sup>/3 hr<sup>2</sup>) of the residual for the (a) Tropics, (b) Subtropics, and (c) extratropics based on three-hourly data. Dashed lines with circles show the correlation among budget terms for each month. The mean and variance are denoted by  $\mu$  and  $\sigma^2$ . The covariance between  $E - P$  and vertically integrated moisture flux divergence (VIMD) is multiplied by  $-1$  for comparison.

for ease of comparison with the other components of variance.

VIMD accounts for most of the seasonal variability of the residual in the extratropics (Figure 4c). This is also true for the Subtropics; however,  $E - P$  contributes a larger fraction of variance during summer than winter (Figure 4b). The VIMD dominates the variability in the Tropics in spring and winter, whereas  $E - P$  becomes almost as important in summer and autumn (Figure 4a). The comparable contribution of  $E - P$  to residual variability in summer in the Tropics and Subtropics is due to the increased variability of evaporation (not shown), which is also reflected by the higher covariance between  $E - P$  and VIMD. The covariance in the extratropics is considerably low throughout, suggesting that the large-scale moisture divergence is the primary driver of the moisture imbalance.

### 2.2.2 | Time-scales of variability

The residual variability analysis in the earlier section was carried out for three-hourly data; that is, weather time-scales. At the same time, we know that for sufficiently long time-scales, the residual approaches zero (except for small re-analysis errors), slow varying climate time-scales. To get a better sense of weather–climate transitions in the moisture budget, we next investigate how the residual variability changes with the averaging time-scale. To do

so, we apply a running-mean filter of lengths from 1 to 365 days and compute the mean residual for each filtered time series. We chose the summer season for this analysis as it includes the tropical rainy season.

The mean summertime residuals decay rapidly, with temporal smoothing (running mean) in all three regions being almost constant for time-scales longer than 20–30 days (Figure 5a). We interpret the flattening of the residual curve as the transition from high-frequency weather to slowly evolving climate variability. To better quantify where this transition occurs in each region, we implement the window-based search method to identify the change point in the residual curve (Truong *et al.*, 2018). The window-based search method computes the discrepancy between two adjacent windows that move along the time series. A change point is detected when the two windows significantly differ in their statistical properties (mean or standard deviations). The change point approach estimates the transition time-scale at 17, 21, and 23 days in the extratropics, Subtropics, and Tropics respectively, with a mean value of 20 days. The transition time-scales in winter are comparable to those in summer (not shown).

It is important to note that these transition time-scales are sensitive to the spatial extent of the region chosen for averaging. In general, the transition time-scales get shorter with increasing area. For example, at sufficiently large spatial scales ( $>2,000$  km), the transition occurs after a few days (not shown). Therefore, we chose the box size such that the transition time-scales based on area-averaged

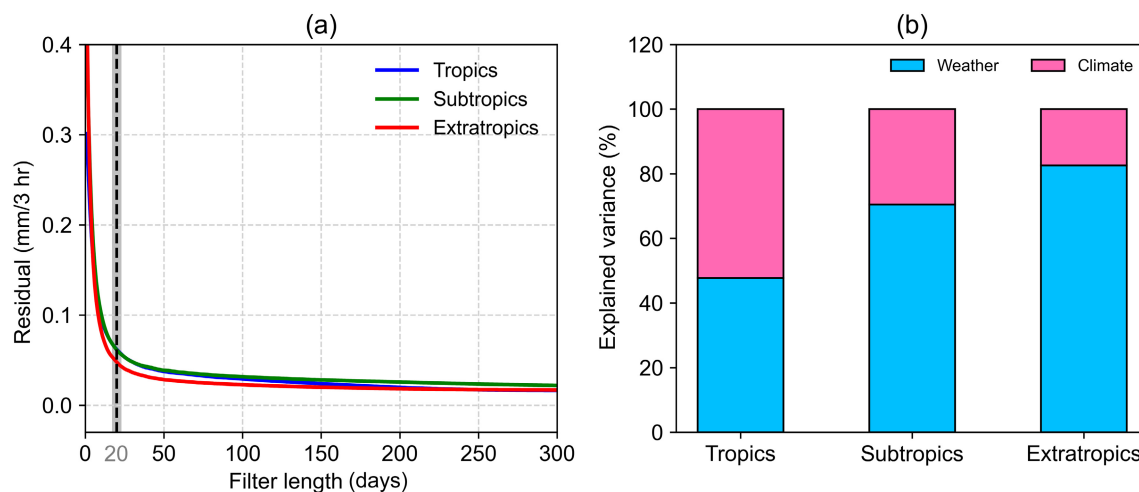


**FIGURE 5** (a) Mean residual (mm/3 hr) for different running mean filters in the Tropics (blue), Subtropics (green), and extratropics (red). (b)  $E - P$  explained variance (%) in the weather (<20 days) and climate (>20 days) time-scales in summer. Low- and high-pass Butterworth filters are applied to partition the total variance into weather and climate components.

$E - P$  time series are not significantly different from those calculated at individual grids and later averaged for the entire region.

Considering 20 days as the weather–climate transition time-scale for all regions, we can quantify the  $E - P$  variance on weather and climate time-scales. We do so by computing the explained variance in weather (<20 days) and climate (>20 days) time-scales by applying a low- and high-pass Butterworth filter. We calculate the explained variance by taking the square of the linear correlation with the unfiltered time series. In summer, weather processes contribute 82% and 71% of the total variance in the extratropics and Subtropics respectively (Figure 5b). The contribution from weather and climate in winter is comparable to that in summer (not shown). In the Tropics, weather and climate are equally important contributors to the total variance. In summer, about 52% (48%) of the variance is observed on the climate (weather) time-scale. The larger contribution of low-frequency climate variability in the Tropics suggests that the annual cycle has much greater control over rainfall than in the Subtropics, as the seasonal cycle of rainfall is pronounced in northern Australia (Nicholls *et al.*, 1982).

To understand the key weather systems responsible for  $E - P$  variability in the weather time-scales, we compute the frequency of different weather systems based on six-hourly weather types datasets (Pepler *et al.*, 2020). The frequency is computed at each grid point for wet ( $E - P < 0$ ) and dry ( $E - P > 0$ ) conditions based on a six-hourly box averaged  $E - P$  time series and then averaged over the desired regions. We categorise the eight weather types from Pepler *et al.* (2020) into four: (a) cyclone/front; (b) thunderstorm; (c) High

(anticyclone circulations); (d) unknown. Weather types such as cyclone, front (cold or warm), cyclone–front, cyclone–thunderstorm, front–thunderstorm, and cyclone–front–thunderstorm are all categorised as cyclone/front for simplicity. The unknown category consists of unconfirmed (fronts and cyclones identified by only one method, as multiple methods were used for fronts and cyclone detection) and unidentified (no weather system is defined). This dataset is primarily designed for midlatitude weather systems and, therefore, is not suitable for the Tropics. Therefore, in the Tropics, we use the six-hourly coherent cyclonic PV anomalies. We compute the frequency of occurrence of PV minimum with a threshold ranging from 0.25 PVU to 1 PVU within the box for wet ( $E - P < 0$ ) and dry ( $E - P > 0$ ) conditions.

Roughly 48% (34%) of the wet (dry) conditions are associated with cyclonic PV anomaly of at least 0.25 PVU in the tropics (Figure 6a). Similar results are obtained for stronger PV anomalies. As tropical low-pressure systems are of common occurrence during summer, it is not surprising that a considerable fraction of dry conditions is also associated with cyclonic PV anomalies.

The frequency distribution of weather types shows that cyclones/fronts are the most relevant weather types for  $E - P$  variability in the Subtropics and extratropics in both seasons (Figure 6b–e). In the Subtropics, during summer, both cyclones/fronts (FRQ ~ 34%) and thunderstorms (FRQ ~ 29%) contribute equally to the wet conditions, whereas cyclones/fronts dominate the variability in winter (Figure 6b,c). High-pressure systems are more frequent in dry conditions in both seasons. In the extratropics, cyclones/fronts are the most important weather systems associated with more than 50% of wet

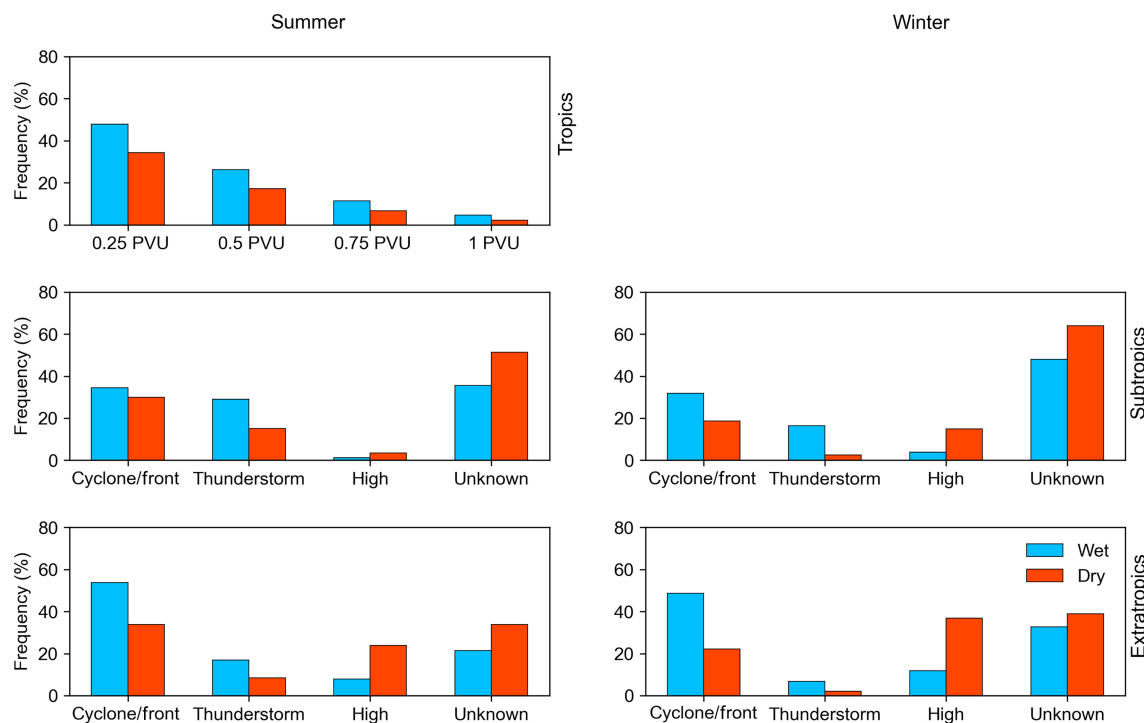


**FIGURE 6** Frequency of three-hourly wet ( $E - P < 0$ ) and dry ( $E - P > 0$ ) conditions in per cent associated with (a) cyclonic potential vorticity anomalies for various thresholds and (b–e) three main midlatitude weather types and unknown three-hourly periods in summer (left) and winter (right). The frequency for wet (dry) conditions is represented by blue (red) bars.

conditions (Figure 6d,e). Thunderstorms share up to 15% of the wet conditions. Cyclones/fronts are also common weather features in dry conditions, but the frequency of high-pressure systems is greatly increased in both seasons, especially in winter (FRQ  $\sim$  37%).

Interestingly, a comparable fraction of dry conditions is associated with cyclonic PV anomalies (cyclones/fronts or thunderstorms) in the Tropics (Subtropics and extratropics). Though the passage of these weather systems could potentially produce necessary circulation anomalies and vertical motion, the lack of moisture within the system leads to little or no rainfall (10–15% of total seasonal rainfall) in dry conditions. To support this inference, we compute the mean of vertically integrated (1,000 hPa to 1 hPa) specific humidity in wet and dry conditions associated with cyclonic PV anomalies in the Tropics and all four weather types in the extratropics/Subtropics. On average, the mean values of vertically integrated specific humidity in wet conditions are 1.5 to 2 times higher than in dry conditions (not shown).

It is noteworthy that a considerable fraction of the weather types falls under the unknown category, which includes unconfirmed or unidentified weather types. About 50% of total six-hourly observations in the unknown category are unidentified, and their proportion is larger in winter than in summer (not shown). Even though a large

fraction of weather types is unconfirmed or unidentified, their contribution to total seasonal rainfall in South Australia is minimal (Pepler *et al.*, 2020, 2021). For example, about 10% (17) and 20% (23) of the seasonal total rainfall in summer (winter) is not associated with any of the four weather types explored in the extratropics and Subtropics (not shown).

### 2.3 | The relationship between $E - P$ and VIMD

The analysis in the previous section showed a very strong covariance of  $E - P$  and VIMD in the Tropics and Subtropics in summer, with very low values in the extratropics. A possible explanation for the low covariance in the extratropics is the presence of a lagged relationship between the two terms. To investigate this further, Figure 7 shows the lag correlations between  $E - P$  and VIMD for all three regions.

One of the distinct behaviours of  $E - P$  variability in the extratropics and Subtropics is its lag relationship with VIMD. In summer, the maximum moisture flux convergence leads to negative  $E - P$  by 12 hr (9 hr) with a correlation coefficient of 0.51 ( $r \sim 0.57$ ) in the extratropics (Subtropics) (Figure 7b,c). In winter, the

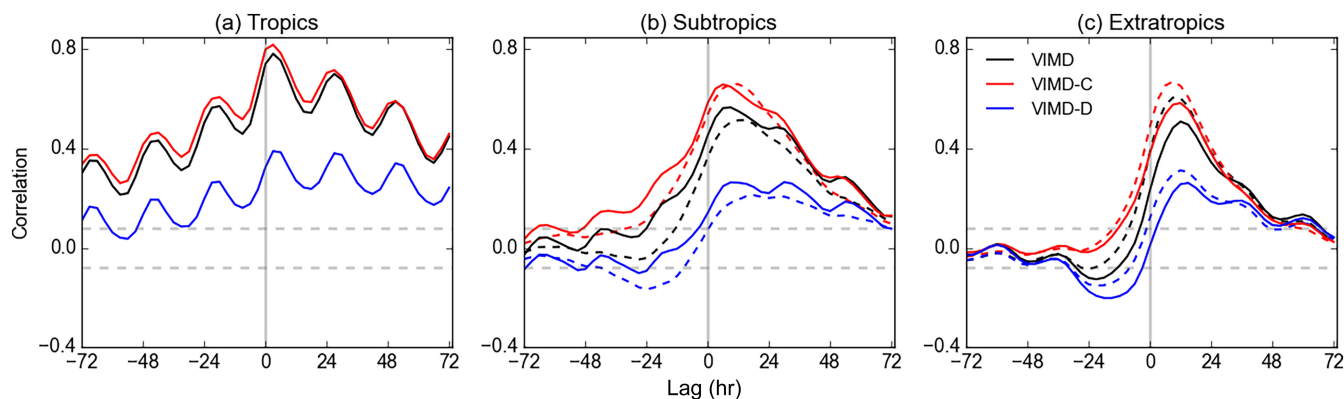


**FIGURE 7** Lag correlation between three-hourly vertically integrated moisture flux divergence (VIMD) (negative values are convergence) and  $E - P$  in summer (solid) and winter (dashed) for the (a) Tropics, (B) Subtropics, and (c) extratropics. The black line represents the total correlation, and the red and blue lines respectively represent the correlation between  $E - P$  and convergence (VIMD-C) and divergence (VIMD-D). A positive correlation is VIMD leading  $E - P$ . Grey dashed lines represent the 99% confidence level.

correlation between  $E - P$  and VIMD is slightly stronger, with a shorter lag in the extratropics ( $r \sim 0.61$ ; lag  $\sim 9$  hr). Interestingly, the correlation coefficients in the Subtropics are slightly lower during winter, and the lags are a little longer ( $r \sim 0.51$ ; lag  $\sim 15$  hr). Even though the differences in the correlation coefficients between summer and winter are smaller, they are statistically significant at the 99% confidence level because of the large sample size. Notably, the correlation in winter does not show a pronounced peak like in summer because of the large variability in the  $E - P$  and VIMD relationship (not shown). This is an interesting issue that needs further exploration and could be a topic for future research.

Unlike the extratropics/Subtropics, the lag between the two budget terms is shorter (lag  $\approx 3$  hr) in the tropics, with a considerably higher correlation coefficient of 0.78 (Figure 7a). Such a nearly in-phase and stronger relationship reflects the typical tropical convective rainfall patterns where the moist air rises due to surface heating and the associated circulation, producing rainfall instantaneously (Davies *et al.*, 2013).

One of the striking characteristics of the  $E - P$ -VIMD relationship is the diurnal cycle. In the Tropics the diurnal cycle of the  $E - P$ -VIMD relationship is quite pronounced. This feature is substantially reduced in the Subtropics and extratropics. The diurnal cycle of rainfall and VIMD is stronger in the Tropics (not shown) because of the stronger diurnal thermal contrast between the ocean and land masses (Sato *et al.*, 2009; Yang & Smith, 2006). The coherence between  $E - P$  and VIMD on a sub-daily time-scale in the Tropics suggests the importance of the diurnal cycle to rainfall variability, compared with the extratropics and Subtropics.

We decompose the total correlation by separating instances of vertically integrated moisture flux

convergence (VIMD-C) and divergence (VIMD-D). The correlation between  $E - P$  and VIMD-C (VIMD-D) is calculated by replacing all the VIMD-D (VIMD-C) values with zeros. The correlation between  $E - P$  and VIMD-C dominates the total correlation in all three regions in both seasons. The positive correlation between  $E - P$  and VIMD-D in the extratropics (Subtropics) suggests that VIMD-D prevails over the region 12–15 hr (18–30 hr) before maximum rainfall, whereas the negative correlation coefficient 18–20 hr (24–27 hr) after the rainfall maximum indicates that rain can still occur within the region of VIMD-D. In the Tropics, VIMD-D plays little or no role, as rainfall variability is primarily contributed by VIMD-C.

The lag correlation also provides a means of quantifying the time-scale of the rainfall events by assessing the decorrelation time. The decorrelation time gets longer from south to north. The life cycle of rainfall events in the extratropics and Subtropics ranges from 2 to 4 days. In the Tropics, rainfall can occur for more than 16 days, with a maximum at day zero.

The monsoon lows are a common synoptic pattern in the Tropics, and these features are observed every 2–3 days (Berry *et al.*, 2012) associated with more than 50% of the wet conditions. Such disturbances along with a moist background state could produce rainfall for several days. On the other hand, rainfall events are short-lived in the extratropics and Subtropics as they are primarily associated with high-frequency midlatitude weather systems such as fronts, cyclones, and thunderstorms.

The lag relationship is further confirmed by time-lag phase composites of  $E - P$  2 days before and after the peak of strong rainfall events. We identify these events as those above the 90th percentile of the three-hourly  $E - P$ —the negative of the right-hand side of Equation (1) time series.

We construct the corresponding composites of VIMD and MSLP for the selected  $E - P$  events. We also apply a 20-day low-pass Butterworth filter to the raw data and compute the composites to compare the large-scale atmospheric features on weather and climate time-scales.

To illustrate the synoptic feature associated with strong rainfall events at weather and climate time-scales, we present the composites for raw and 20-day low-pass filtered data 1 day before the heavy event, the day of the event, and the day after the event (Figure 8). We apply a 20-day low-pass filter to demonstrate and compare the large-scale features associated with a slow-evolving background state. For the raw data, we observe clear eastward-propagating signals of VIMD followed by low  $E - P$  (more rainfall) in the extratropics (Figure 8m-o). In contrast, a less pronounced eastward propagation is also apparent in the Subtropics (Figure 8g-i). In the Tropics, the same synoptic pattern persists 1 day before the event, the day of the event, and 1 day after the event (Figure 8a-c).

The raw composite of MSLP in the extratropics shows a low-pressure trough across southeast Australia with a low-pressure system on the day of the event (Figure 8n), a typical synoptic pattern of an extratropical cyclone. The synoptic patterns for the Subtropics show a trough associated with a low-pressure system southwest of the subtropical box (Figure 8h). In both cases, the maximum of negative VIMD and  $E - P$  is in the warm sector of the trough. In the Tropics, heavy rainfall events seem to be associated with the tropical low-pressure system or tropical cyclones with a low-pressure system over the tropical box (Figure 8b).

The low-frequency composites show considerable differences in the extratropics (Figure 8p-r) and Subtropics (Figure 8j-l), whereas in the Tropics (Figure 8d-f) a slightly weaker version of a similar synoptic pattern persists. The MSLP pattern is very similar for all three regions for the filtered data and represents the mean background state. The comparable patterns with considerable magnitude in the Tropics between raw and filtered composites reflect the importance of a slowly varying background state, unlike the extratropics and Subtropics, where both the pattern and magnitudes differ significantly.

## 2.4 | The moisture budget in wet and dry years

We apply the moisture budget approach to understand how the  $E - P$ -VIMD relationship changes between wet and dry years for the two extended seasons used here. We chose the five wettest and driest summers and winters in our dataset based on seasonal  $E - P$  anomalies averaged

over the relevant region. The association between  $E - P$  and VIMD in wet years is stronger in both summer and winter in all three regions. The correlation coefficients of 0.58 (0.45), 0.63 (0.44), and 0.64 (0.47) are observed in wet (dry) years for summer in the extratropics, Subtropics, and Tropics respectively. The respective correlation coefficients for winter in the extratropics and Subtropics are 0.66 (0.46) and 0.64 (0.39). These correlation coefficients are computed from three-hourly time series. To better understand these relationships, we construct a two-dimensional frequency distribution of  $E - P$  and VIMD (Figure 9). Note that correlation coefficients and the two-dimensional frequency distribution are computed after adjusting the lag relationship between  $E - P$  and VIMD by shifting the time series.

The two budget terms are better related in the Tropics, with a relatively smaller spread of the frequency distribution and a more obvious linear relationship (Figure 9a). The frequency distribution is wider and somewhat non-linear in the extratropics and Subtropics (Figure 9b,c). In the extratropics and Subtropics, a considerable fraction of positive  $E - P$  (more evaporation) events is associated with strong moisture flux divergence. This feature is less apparent in the Tropics, consistent with a weak correlation between  $E - P$  and moisture flux. The shape of the frequency distribution for the extratropics and Subtropics in winter is similar to that in summer (Figure 9g,h). However, the width of the distribution is reduced, consistent with a better correlation between  $E - P$  and VIMD, as discussed earlier.

The difference in frequency distribution between wet and dry years (wet minus dry), by definition, shows an overall increase in negative  $E - P$  (more rainfall) events that are linked to enhanced moisture flux convergence in all three regions (Figure 9d-f). However, there is also an increase in the frequency of strong positive  $E - P$  (more evaporation) events, corresponding to moisture flux divergence in the extratropics and partly in the Subtropics. These features are also present in winter in both regions (Figure 9i,j). The frequency distribution of  $E - P$  and lower tropospheric wind divergence shows a similar pattern, suggesting that both wind convergence and divergence are enhanced during wet years in the extratropics and Subtropics (Supporting Information Figure S2).

The difference in frequency distribution between wet and dry years in the Tropics shows an overall increase in negative  $E - P$  (more rainfall) associated with increased moisture flux convergence and a decrease in positive  $E - P$  (less evaporation) associated with reduced moisture flux divergence. These changes are attributed to increased column-integrated specific humidity and an increased frequency of lower tropospheric wind convergence during the wet season (Supporting Information Figure S2).

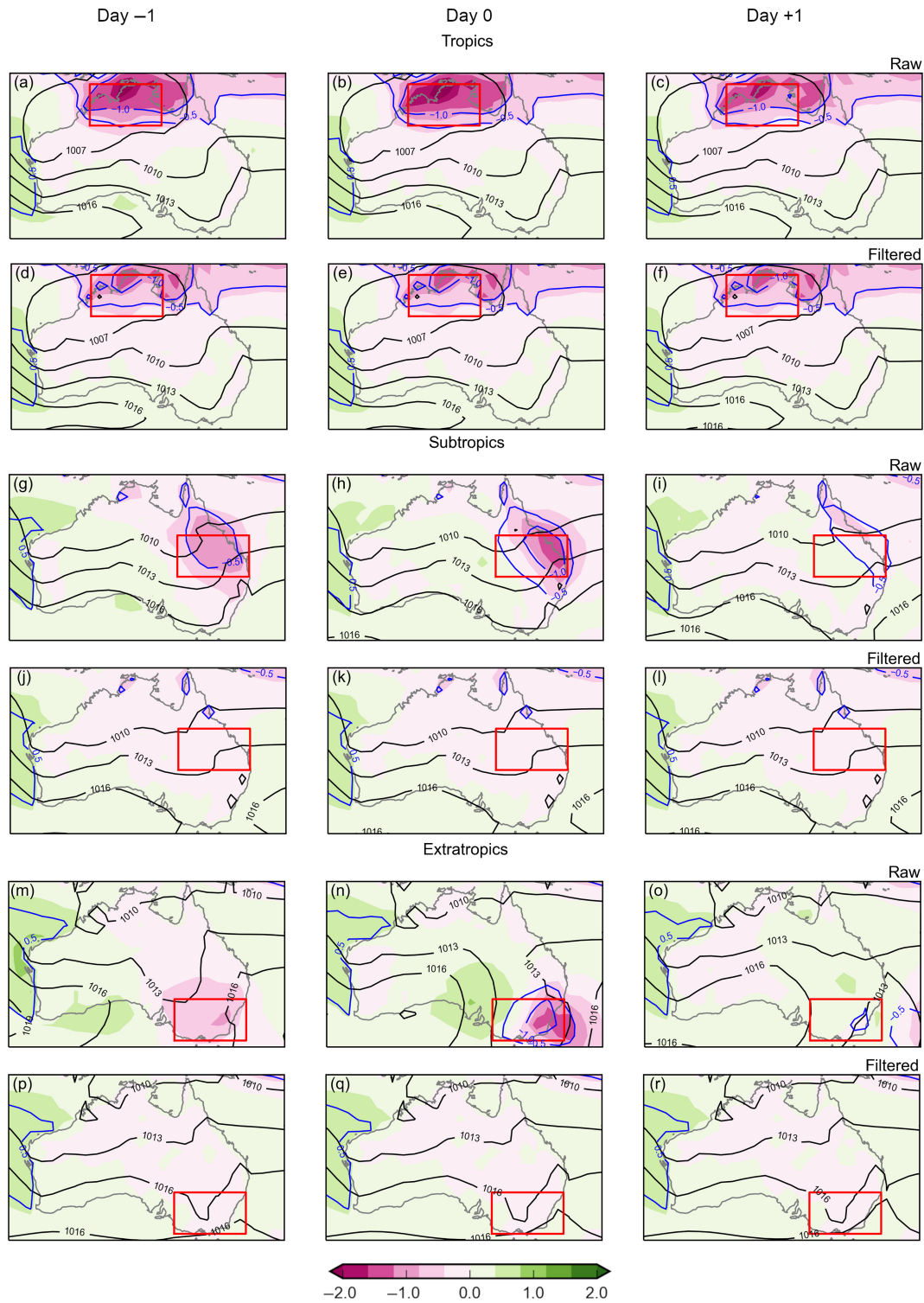


**FIGURE 8** Composites of vertically integrated moisture flux divergence (shaded; mm/3 hr),  $E - P$  (blue contours; mm/3 hr, contour interval 1, beginning at  $-1$ ), and sea-level pressure (black contours; hPa, contour interval 3, beginning at 1,007 hPa) for raw and 20-day low-pass filtered data. The composites are computed from three-hourly rainfall with amplitude greater than the 90th percentile for 1 day before the heavy event, the day of the event, and the day after the event.

### 3 | SUMMARY

We investigate the rainfall variability in three regions across Australia based on the atmospheric moisture

budget using the three-hourly ERA5 and ERA5-Land datasets from 1979 to 2022. Climatologically, the moisture budget virtually closes for most of Australia except in regions with complex topography,

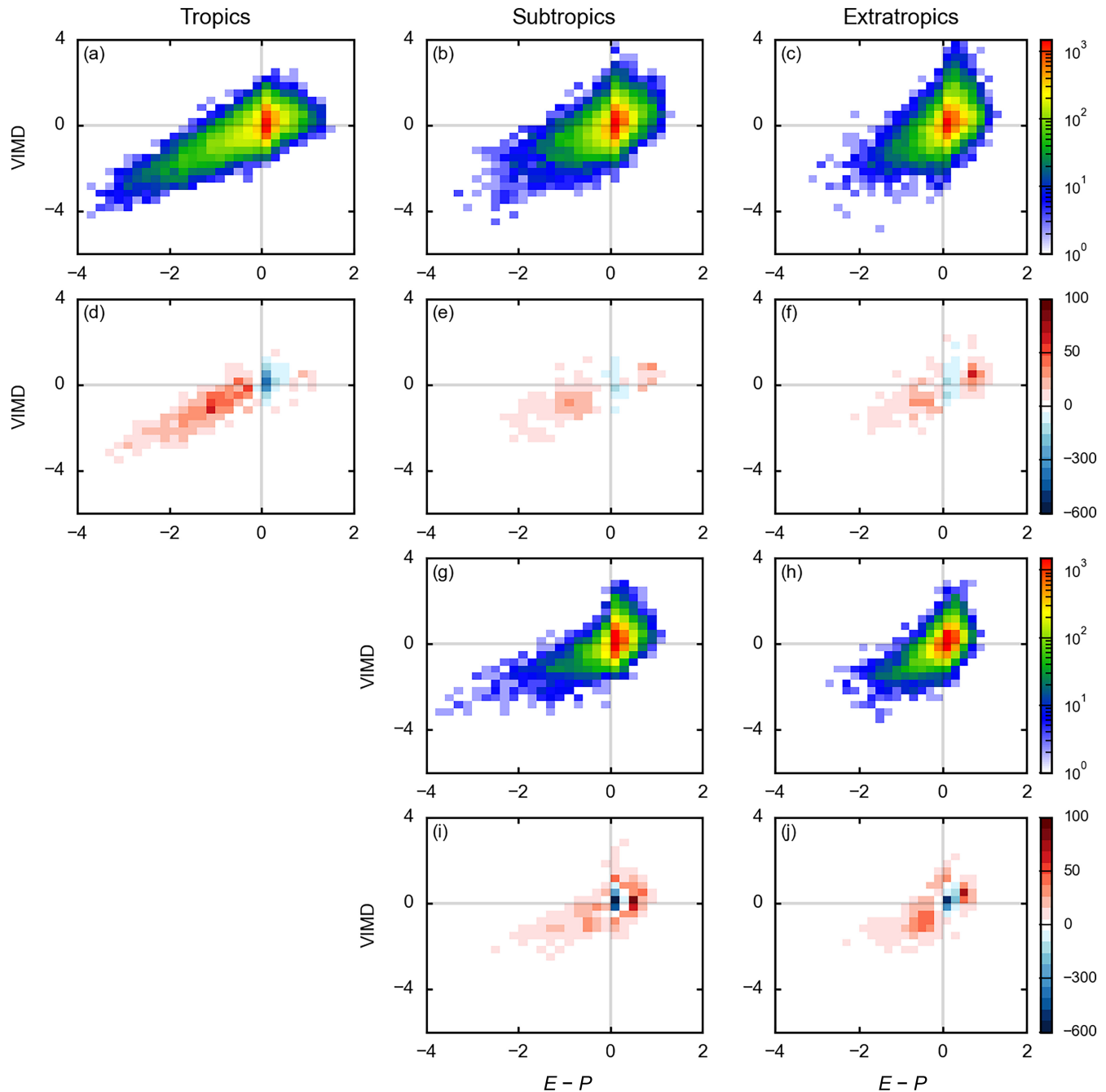


**FIGURE 9** Two-dimensional frequency distribution of  $E - P$  and vertically integrated moisture flux divergence (VIMD) based on three-hourly data for (a–f) summer and (g–j) winter. The total joint distribution (a–c, g, h) is represented on a log scale, and the difference between wet and dry years (wet minus dry; d–f, i, j) is represented by a nonlinear scale. The values represented are the frequency of three-hourly events in each bin.

such as the mountainous southeast and southwest Australia.

On three-hourly time-scales, the variability of the VIMD is twice that of  $E - P$ , due to the large sub-daily variability of the VIMD. This difference is even larger along the northern and eastern coastlines because of the larger wind and moisture variability associated with land–ocean interaction. On these short weather time-scales, the residual

term of the moisture budget is smaller in winter in the extratropics and in summer in the Subtropics and Tropics. The moisture imbalance is dominated by the variability in VIMD in the extratropics. This suggests that moisture availability is largely determined by the import and export of moisture. In contrast,  $E - P$  and the covariance between  $E - P$  and VIMD contribute equally to the moisture imbalance in the Tropics and Subtropics, highlighting

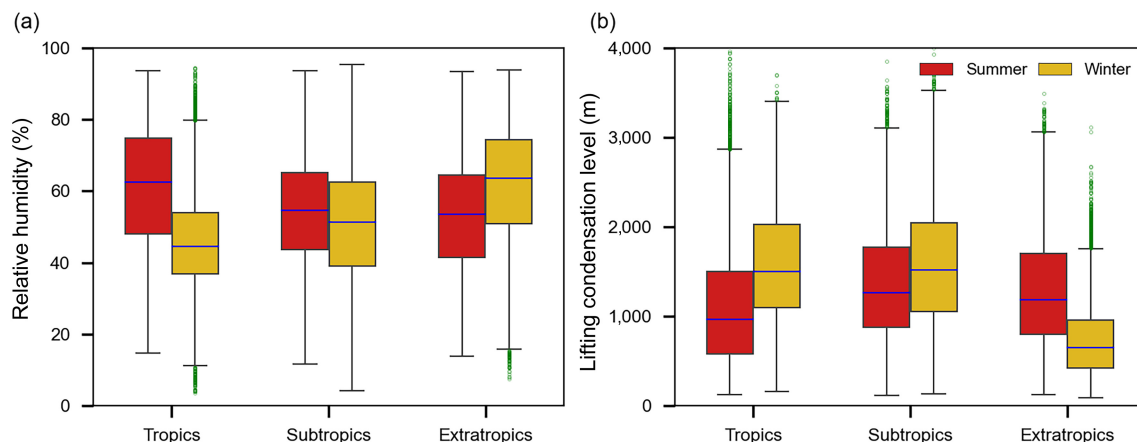


**FIGURE 10** Box plot of three-hourly (a) relative humidity (%) and (b) lifting condensation level (m) in summer (red) and winter (yellow). The blue line represents the median; boxes extend from the 25th to the 75th percentiles. Whiskers represent the 1.5 interquartile range of the 25th and the 75th percentiles. Green dots denote values outside the 1.5 interquartile range.

the relative role of evaporation and moisture import/export and their interactions in these regions.

The time-scale that differentiates weather and climate in Australia is roughly 20 days. Weather systems dominate the total  $E - P$  variability in the extratropics/Subtropics. In contrast, both weather and climate-induced variability are important in the Tropics. On the weather time-scale, cyclones/fronts and thunderstorms are the main weather systems for wet conditions in the Subtropics and extratropics. These weather features are also associated with dry conditions, but the occurrence of high-pressure systems is equally important, especially in the extratropics. In the Tropics, cyclonic PV anomalies dominate  $E - P$  variability on weather time-scales. These cyclonic PV anomalies represent tropical disturbances (monsoon lows) or tropical cyclones, which are the key synoptic weather patterns in this region (King *et al.*, 2014).

The climate (variability greater than 20 days) includes monthly or seasonal mean and its variability from intraseasonal to interannual and longer time-scales. In Australia, the relevant climate modes are the Madden–Julian Oscillation, southern annular mode, El Niño–Southern Oscillation, Indian Ocean dipole, and the interdecadal Pacific oscillation. Acting on different time-scales, these climate modes modulate the background state of evaporation or precipitation by changing the atmospheric temperature, large-scale circulation, and moisture availability (Borowiak *et al.*, 2023; Dao *et al.*, 2023; Ghelani *et al.*, 2017; Heidemann *et al.*, 2023; Liguori *et al.*, 2022; McKay *et al.*, 2023; Tozer *et al.*, 2023). Presumably, these changes in the background state change the intensity and frequency of the weather systems, which ultimately produce precipitation. A comprehensive assessment of how these different climate drivers impact the rainfall

variability in these three regions is therefore essential and needs further study.

The  $E - P$ -VIMD relationship in the Tropics is distinct from the remaining two regions. In the Tropics, the  $E - P$ -VIMD relationship is stronger and the lags are shorter, whereas in the extratropics and Subtropics the VIMD leads  $E - P$  by 9–15 hr. The summertime background atmospheric state is quite moist, with higher relative humidity in the Tropics (Figure 10a). Therefore, the air within the box saturates quickly and condenses into rainfall. This is confirmed by the lower lifting condensation level in the Tropics (Figure 10b). However, in the Subtropics and extratropics, the rainfall variability is largely driven by large-scale weather systems, especially midlatitude cyclones and fronts. These weather systems typically propagate from west to east in southern Australia (Figure 8), which could explain such a lag relationship. The seasonal differences in lag between VIMD and  $E - P$ , particularly in the extratropics, are due to the different background atmospheric states. The relative humidity is much lower in summer than in winter (Figure 10a), so it takes more time for the air to be saturated within the box and that is why the lag is slightly longer with a relatively weaker correlation in summer. The opposite is true in the Subtropics.

The importance of weather systems in the extratropics and Subtropics is also reflected in the typical time-scale of rainfall events. Typical rainfall events in the extratropics and Subtropics show a time-scale of 2–4 days, consistent with the typical time-scales for weather systems. In contrast, light to moderate rain lasts for over 16 days in the Tropics, with a short episode of heavy rainfall. This is a manifestation of superimposed tropical cyclones or low-pressure systems onto the mean background state, a

combined effect of a slow-evolving mean background state and high-frequency weather systems.

The relationship between  $E - P$  and VIMD is stronger during wet years in all three regions, with increased frequency of rainfall that is linked to more frequent moisture flux convergence. However, in the extratropics and Subtropics there is also an increase in the frequency of positive  $E - P$  events that are associated with increased moisture flux divergence. Such an increase in moisture flux convergence and divergence during wet years is perhaps linked to the enhancement of midlatitude weather systems with regions of ascent (convergence) and subsidence (divergence). However, these are just speculations at this stage, and further study is needed to test this hypothesis.

This study contributes to understanding rainfall variability from a different perspective, where we connect weather and climate based on the atmospheric moisture budget. Our findings on the weather climate time-scale, quantification of weather- and climate-related  $E - P$  variability, and the dynamical relationship between  $E - P$  and VIMD in different seasons or wet and dry years provide new insights on rainfall variability that are not only relevant for fundamental understanding but also in assessing rainfall response to future climate change in Australia. The next step in assessing the potential future of rainfall variability is to understand whether current climate models can capture the key observed features of the moisture budget and the dynamic relationship between  $E - P$  and VIMD in the different regions. Once some confidence in the model's performance is established, future changes in the moisture budget can be examined to understand potential changes in the weather-climate connection and their consequences.

#### ACKNOWLEDGEMENTS

We would like to thank Acacia Pepler for providing the Australian weather types datasets. This work is supported by the Australian Research Council (grant number-DP200102954). Open access publishing facilitated by Monash University, as part of the Wiley - Monash University agreement via the Council of Australian University Librarians.

#### FUNDING INFORMATION

The funding for this study is provided by the Australian Research Council (grant number-DP200102954).

#### DATA AVAILABILITY STATEMENT

Data sharing does not apply to this article as no new data were created. The weather types and cyclonic PV datasets used in this study are obtained from the original authors (Acacia Pepler and Michael Barnes). These datasets are available with the permission of the authors.

#### ORCID

Sunil Kumar Pariyar  <https://orcid.org/0000-0002-6477-3358>

Giovanni Liguori  <https://orcid.org/0000-0002-1617-350X>

Michael A. Barnes  <https://orcid.org/0000-0001-8056-8875>

#### REFERENCES

- Alexander, L.V. & Arblaster, J.M. (2017) Historical and projected trends in temperature and precipitation extremes in Australia in observations and CMIP5. *Weather and Climate Extremes*, 15, 34–56.
- Ashok, K., Guan, Z. & Yamagata, T. (2003) Influence of the Indian Ocean dipole on the Australian winter rainfall. *Geophysical Research Letters*, 30, 1821.
- Ashok, K., Nakamura, H. & Yamagata, T. (2007) Impacts of ENSO and Indian Ocean dipole events on the southern hemisphere storm-track activity during austral winter. *Journal of Climate*, 20, 3147–3163.
- Barnes, M.A., King, M., Reeder, M. & Jakob, C. (2023) The dynamics of slow-moving coherent cyclonic potential vorticity anomalies and their links to heavy rainfall over the eastern seaboard of Australia. *Quarterly Journal of the Royal Meteorological Society*, 149, 2233–2251.
- Berry, G.J., Reeder, M.J. & Jakob, C. (2012) Coherent synoptic disturbances in the Australian monsoon. *Journal of Climate*, 25, 8409–8421.
- Borowiak, A., King, A. & Lane, T. (2023) The link between the madden-Julian oscillation and rainfall trends in Northwest Australia. *Geophysical Research Letters*, 50, e2022GL101799.
- Brown, J.R., Moise, A.F., Colman, R. & Zhang, H. (2016) Will a warmer world mean a wetter or drier Australian monsoon? *Journal of Climate*, 29, 4577–4596.
- Brown, J.R., Moise, A.F. & Colman, R.A. (2017) Projected increases in daily to decadal variability of Asian-Australian monsoon rainfall. *Geophysical Research Letters*, 44, 5683–5690.
- Chen, G., Norris, J., Neelin, J.D., Lu, J., Leung, L.R. & Sakaguchi, K. (2019) Thermodynamic and dynamic mechanisms for hydrological cycle intensification over the full probability distribution of precipitation events. *Journal of the Atmospheric Sciences*, 76, 497–516.
- Chiew, F.H., Piechota, T.C., Dracup, J.A. & McMahon, T.A. (1998) El Nino/southern oscillation and Australian rainfall, streamflow and drought: links and potential for forecasting. *Journal of Hydrology*, 204, 138–149.
- Cowan, T., Van Rensch, P., Purich, A. & Cai, W. (2013) The association of tropical and extratropical climate modes to atmospheric blocking across southeastern Australia. *Journal of Climate*, 26, 7555–7569.
- Dao, T.L., Vincent, C.L. & Lane, T.P. (2023) Multiscale influences on rainfall in Northeast Australia. *Journal of Climate*, 36, 5989–6006.
- Davies, L., Jakob, C., May, P., Kumar, V. & Xie, S. (2013) Relationships between the large-scale atmosphere and the small-scale convective state for Darwin, Australia. *Journal of Geophysical Research: Atmospheres*, 118, 11534–11545.

- Dey, R., Lewis, S.C., Arblaster, J.M. & Abram, N.J. (2019) A review of past and projected changes in Australia's rainfall. *Wiley Interdisciplinary Reviews: Climate Change*, 10, e577.
- Dowdy, A.J. & Catto, J.L. (2017) Extreme weather caused by concurrent cyclone, front and thunderstorm occurrences. *Scientific Reports*, 7, 40359.
- Fierro, A.O. & Leslie, L.M. (2013) Links between central west Western Australian rainfall variability and large-scale climate drivers. *Journal of Climate*, 26, 2222–2246.
- Ghelani, R.P.S., Oliver, E.C.J., Holbrook, N.J., Wheeler, M.C. & Klotzbach, P.J. (2017) Joint modulation of intraseasonal rainfall in tropical Australia by the Madden-Julian oscillation and El Niño-southern oscillation. *Geophysical Research Letters*, 44, 10754–10761.
- Grose, M.R., Narsey, S., Delage, F., Dowdy, A.J., Bador, M., Boschat, G. et al. (2020) Insights from CMIP6 for Australia's future climate. *Earth's Futures*, 8, e2019EF001469.
- Hauser, S., Grams, C.M., Reeder, M.J., Mcgregor, S., Fink, A.H. & Quinting, J.F. (2020) A weather system perspective on winter-spring rainfall variability in southeastern Australia during El Niño. *Quarterly Journal of the Royal Meteorological Society*, 146, 2614–2633.
- Heidemann, H., Cowan, T., Henley, B.J., Ribbe, J., Freund, M. & Power, S. (2023) Variability and long-term change in Australian monsoon rainfall: a review. *WIREs Climate Change*, 14, e823.
- Hendon, H.H., Thompson, D.W.J. & Wheeler, M.C. (2007) Australian rainfall and surface temperature variations associated with the southern hemisphere annular mode. *Journal of Climate*, 20, 2452–2467.
- Hersbach, H., Bell, B., Berrisford, P., Hirahara, S., Horányi, A., Muñoz-Sabater, J. et al. (2020) The ERA5 global reanalysis. *Quarterly Journal of the Royal Meteorological Society*, 146, 1999–2049.
- Hoang, L.P., Reeder, M.J., Berry, G.J. & Schwendike, J. (2016) Coherent potential vorticity maxima and their relationship to extreme summer rainfall in the Australian and north African tropics. *Journal of Southern Hemisphere Earth Systems Science*, 66, 424–441.
- Holgate, C., Evans, J., Van Dijk, A., Pitman, A. & Di Virgilio, G. (2020) Australian precipitation recycling and evaporative source regions. *Journal of Climate*, 33, 8721–8735.
- King, A.D., Klingaman, N.P., Alexander, L.V., Donat, M.G., Jourdain, N.C. & Maher, P. (2014) Extreme rainfall variability in Australia: patterns, drivers, and predictability. *Journal of Climate*, 27, 6035–6050.
- Klingaman, N.P. (2012) *Rainfall in Queensland: part 1: a literature survey of key rainfall drivers in Queensland Australia: rainfall variability and change*. Brisbane, Australia: Queensland Government.
- Li, Z., Cai, W. & Lin, X. (2016) Dynamics of changing impacts of tropical Indo-Pacific variability on Indian and Australian rainfall. *Scientific Reports*, 6, 31767.
- Liguori, G., Mcgregor, S., Singh, M., Arblaster, J. & Di Lorenzo, E. (2022) Revisiting ENSO and IOD contributions to Australian precipitation. *Geophysical Research Letters*, 49, e2021GL094295.
- Lim, E.-P., Hendon, H.H., Zhao, M. & Yin, Y. (2017) Inter-decadal variations in the linkages between ENSO, the IOD and south-eastern Australian springtime rainfall in the past 30 years. *Climate Dynamics*, 49, 97–112.
- Mapes, B.E., Warner, T.T., Xu, M. & Negri, A.J. (2003) Diurnal patterns of rainfall in northwestern South America. Part I: observations and context. *Monthly Weather Review*, 131, 799–812.
- Mayer, J., Mayer, M. & Haimberger, L. (2021) Consistency and homogeneity of atmospheric energy, moisture, and mass budgets in ERA5. *Journal of Climate*, 34, 3955–3974.
- McKay, R.C., Boschat, G., Rudeva, I., Pepler, A., Purich, A., Dowdy, A. et al. (2023) Can southern Australian rainfall decline be explained? A review of possible drivers. *WIREs Climate Change*, 14, e820.
- Moron, V., Barbero, R., Evans, J.P., Westra, S. & Fowler, H.J. (2019) Weather types and hourly to multiday rainfall characteristics in tropical Australia. *Journal of Climate*, 32, 3983–4011.
- Muñoz-Sabater, J., Dutra, E., Agustí-Panareda, A., Albergel, C., Arduini, G., Balsamo, G. et al. (2021) ERA5-land: a state-of-the-art global reanalysis dataset for land applications. *Earth System Science Data*, 13, 4349–4383.
- Narsey, S., Brown, J., Colman, R., Delage, F., Power, S., Moise, A. et al. (2020) Climate change projections for the Australian monsoon from CMIP6 models. *Geophysical Research Letters*, 47, e2019GL086816.
- Newman, M., Kiladis, G.N., Weickmann, K.M., Ralph, F.M. & Sardeshmukh, P.D. (2012) Relative contributions of synoptic and low-frequency eddies to time-mean atmospheric moisture transport, including the role of atmospheric rivers. *Journal of Climate*, 25, 7341–7361.
- Nicholls, N., McBride, J.L. & Ormerod, R.J. (1982) On predicting the onset of the Australian wet season at Darwin. *Monthly Weather Review*, 110(1), 14–17.
- Norris, J., Chen, D., Hall, A. & Thackeray, C.W. (2022) Moisture-budget drivers of global projections of meteorological drought from multiple GCM large ensembles. *Journal of Geophysical Research: Atmospheres*, 127, e2022JD037745.
- Norris, J., Chen, G. & Li, C. (2020) Dynamic amplification of subtropical extreme precipitation in a warming climate. *Geophysical Research Letters*, 47, e2020GL087200.
- Norris, J., Chen, G. & Neelin, J.D. (2019a) Changes in frequency of large precipitation accumulations over land in a warming climate from the CESM large ensemble: the roles of moisture, circulation, and duration. *Journal of Climate*, 32, 5397–5416.
- Norris, J., Chen, G. & Neelin, J.D. (2019b) Thermodynamic versus dynamic controls on extreme precipitation in a warming climate from the community earth system model large ensemble. *Journal of Climate*, 32, 1025–1045.
- Pepler, A.S., Di Luca, A. & Evans, J.P. (2018) Independently assessing the representation of midlatitude cyclones in high-resolution reanalyses using satellite observed winds. *International Journal of Climatology*, 38, 1314–1327.
- Pepler, A.S., Dowdy, A.J. & Hope, P. (2021) The differing role of weather systems in southern Australian rainfall between 1979–1996 and 1997–2015. *Climate Dynamics*, 56, 2289–2302.
- Pepler, A.S., Dowdy, A.J., Van Rensch, P., Rudeva, I., Catto, J.L. & Hope, P. (2020) The contributions of fronts, lows and thunderstorms to southern Australian rainfall. *Climate Dynamics*, 55, 1489–1505.
- Pitman, A. & Perkins, S. (2008) Regional projections of future seasonal and annual changes in rainfall and temperature over Australia based on skill-selected AR4 models. *Earth Interactions*, 12, 1–50.

- Power, S., Casey, T., Folland, C., Colman, A. & Mehta, V. (1999) Inter-decadal modulation of the impact of ENSO on Australia. *Climate Dynamics*, 15, 319–324.
- Risbey, J.S., Pook, M.J., Mcintosh, P.C., Wheeler, M.C. & Hendon, H.H. (2009) On the remote drivers of rainfall variability in Australia. *Monthly Weather Review*, 137, 3233–3253.
- Sato, T., Miura, H., Satoh, M., Takayabu, Y.N. & Wang, Y. (2009) Diurnal cycle of precipitation in the tropics simulated in a global cloud-resolving model. *Journal of Climate*, 22, 4809–4826.
- Seager, R., Neelin, D., Simpson, I., Liu, H., Henderson, N., Shaw, T. et al. (2014) Dynamical and thermodynamical causes of large-scale changes in the hydrological cycle over North America in response to global warming. *Journal of Climate*, 27, 7921–7948.
- Spensberger, C., Reeder, M.J., Spengler, T. & Patterson, M. (2020) The connection between the southern annular mode and a feature-based perspective on southern hemisphere midlatitude winter variability. *Journal of Climate*, 33, 115–129.
- Suppiah, R. (1992) The Australian summer monsoon: a review. *Progress in Physical Geography: Earth and Environment*, 16, 283–318.
- Ting, M., Seager, R., Li, C., Liu, H. & Henderson, N. (2018) Mechanism of future spring drying in the southwestern United States in CMIP5 models. *Journal of Climate*, 31, 4265–4279.
- Tozer, C.R., Risbey, J.S., Monselesan, D.P., Pook, M.J., Irving, D., Ramesh, N. et al. (2023) Impacts of ENSO on Australian rainfall: what not to expect. *Journal of Southern Hemisphere Earth Systems Science*, 73, 77–81.
- Trenberth, K.E. & Guillemot, C.J. (1995) Evaluation of the global atmospheric moisture budget as seen from analyses. *Journal of Climate*, 8, 2255–2272.
- Truong, C., Oudre, L. & Vayatis, N. (2018) Ruptures: change point detection in python. arXiv preprint arXiv:1801.00826.
- Wilson, L., Manton, M.J. & Siems, S.T. (2013) Relationship between rainfall and weather regimes in south-eastern Queensland, Australia. *International Journal of Climatology*, 33, 979–991.
- Yang, S. & Smith, E.A. (2006) Mechanisms for diurnal variability of global tropical rainfall observed from TRMM. *Journal of Climate*, 19, 5190–5226.
- Zhang, H., Wang, B., Li Liu, D., Zhang, M., Feng, P., Cheng, L. et al. (2019) Impacts of future climate change on water resource availability of eastern Australia: a case study of the Manning River basin. *Journal of Hydrology*, 573, 49–59.

## SUPPORTING INFORMATION

Additional supporting information can be found online in the Supporting Information section at the end of this article.

**How to cite this article:** Pariyar, S.K., Liguori, G., Jakob, C., Singh, M.S., Reeder, M.J. & Barnes, M.A. (2024) A moisture budget perspective on Australian rainfall variability. *Quarterly Journal of the Royal Meteorological Society*, 150(763), 3511–3526. Available from: <https://doi.org/10.1002/qj.4778>